Carbon 133 (2018) 384–389

Contents lists available at ScienceDirect

Carbon

journal homepage: www.elsevier.com/locate/carbon

The creation of hollow walls in carbon nanotubes for high-performance lithium ion batteries

Zhiyong Pan, Hao Sun, Jian Pan, Jing Zhang, Bingjie Wang*, Huisheng Peng**

State Key Laboratory of Molecular Engineering of Polymers, Department of Macromolecular Science and Laboratory of Advanced Materials, Fudan University, Shanghai 200438, China

ARTICLE INFO

Article history:
Received 18 October 2017
Received in revised form
13 February 2018
Accepted 10 March 2018
Available online 12 March 2018

ABSTRACT

Although high mechanical and electronic properties have made carbon nanotube (CNT) a promising active material for lithium ion batteries, the relatively low theoretical specific capacity (372 mAh g^{-1}) of CNT has hindered its application. Here we have developed a general and efficient template strategy in synthesizing a new family of CNTs with controllable hollow walls and explored their promising applications in LIBs. The hollow structure formed between CNT core and nitrogen-doped graphene shell can be effectively used for lithium storage, and a reversible specific capacity of 635 mAh g^{-1} was achieved as anode material in LIB. Interestingly, the hollow structure has been further incorporated with silicon to offer even higher specific capacity of 930 mAh g^{-1} with good cyclic stability.

1. Introduction

Modern electronics have witnessed the emergence of various energy storage devices that are widely used in our daily life [1–4]. Particularly, lithium ion batteries (LIBs) have attracted broad interests from both academy and industry due to the demonstrated high performances [5–7]. Among a broad range of active materials, carbon nanotube (CNT) has been mostly explored as a promising one due to its high mechanical and electronic properties [8–10]. However, based on the lithium storage mechanism, i.e., one lithium atom for six carbon atoms, a relatively low specific capacity is available for CNTs, which largely hinders their applications as high-performance anode materials for LIBs [11–16].

The specific capacity of CNTs may also be affected by its morphology [17–20], and the design of hollow structures in their walls is expected to obviously enhance their energy storage capability because the resulting hollow space may store more charges and greatly increase stability by accommodating large volume variation during charge and discharge. It is necessary while remains challenging to synthesize such CNTs with hollow walls based on the available synthetic approaches.

In this Communication, we have developed a general and efficient template strategy in synthesizing a new family of CNTs (Fig. 1a) with controllable hollow walls and explored their promising applications in LIBs. The hollow structure formed between CNT core and nitrogen-doped graphene shell can be effectively used for lithium storage, so the novel CNTs (denoted as HNCNTs) showed a reversible specific capacity of 635 mAh g^{-1} as anode material in LIB. In addition, the hollow structure also provided ideal platform for incorporation of active materials such as silicon, so the silicon volume change can be well accommodated during charge and discharge, which produced even much higher specific capacity of 930 mAh g^{-1} with good cyclic stability.

2. Experimental section

The synthesis of spinnable CNT arrays was discussed previously [21] and further summarized in the Supporting Information. Aligned CNT sheets were dry-drawn from spinnable CNT arrays and transferred to a curved polytetrafluoroethylene board that was kept suspending. After the deposition of Al_2O_3 on both sides of a CNT sheet by electron beam evaporation, nitrogen-doped graphene layers were grown on the outer surface of Al_2O_3 layer through chemical vapor deposition. The Al_2O_3-coated CNT sheet was first transferred to a silicon wafer with two ends fixed, then the chemical vapor deposition process was applied with Ar (110 sccm) and H_2 (10 sccm) as the carrying gas. When the temperature reached 1060 °C, Ar (40 sccm) and CH_3CN were further introduced

---

* Corresponding author.
** Corresponding author.
E-mail addresses: wangbingjie@fudan.edu.cn (B. Wang), penghs@fudan.edu.cn (H. Peng).

https://doi.org/10.1016/j.carbon.2018.03.021

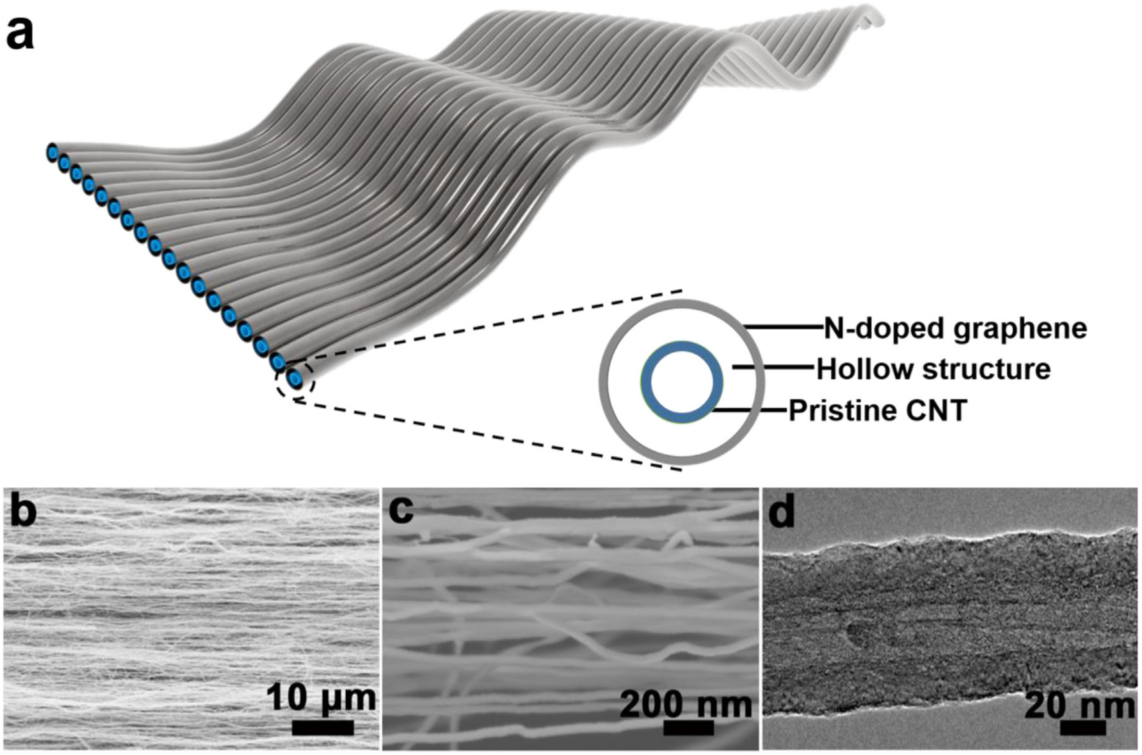

Fig. 1. (a) Schematic illustration to the structure of the aligned HNCNTs. (b) Scanning electron microscope (SEM) image of an aligned CNT sheet. (c) SEM image of a nitrogen-doped graphene/Al_2O_3/CNT film. (d) Transmission electron microscope (TEM) image of nitrogen-doped graphene/Al_2O_3/CNT after HF etching. Thickness of Al_2O_3 in c and d, 10 nm. (A colour version of this figure can be viewed online.)

to the tube furnace, and the reaction time was controlled from 5 to 30 min to synthesize nitrogen-doped graphene shells with different thicknesses. The obtained samples were then immersed in HF (10 vol%) for 24 h to thoroughly remove the Al_2O_3 layer. The obtained samples were then washed with deionized water for three times and dried in vacuum oven at 80 °C for 24 h. In the case of Si-incorporated HNCNTs, Si was deposited on both sides of the CNT sheet before the deposition of Al_2O_3. HCl instead of HF was used to etch Al_2O_3 layer. All the other experimental conditions were kept the same to the HNCNTs.

3. Results and discussion

Spinnable CNT arrays were synthesized *via* chemical vapor deposition using Fe/Al_2O_3 as catalysts. The as-synthesized CNTs were multi-walled with an average diameter of ~15 nm. Aligned CNT sheets could be then continuously drawn from aligned CNT arrays (Fig. 1b), followed by deposition of Al_2O_3 onto their surfaces through electron beam evaporation. Another nitrogen-doped graphene layer was then grown onto the surface also by chemical vapor deposition but at a higher temperature of 1060 °C (Figs. 1c and S1). Based on the XPS test, the atomic content of nitrogen was ~5% as shown in Fig. S1. The graphitization of the re-grown layer can be confirmed by high-resolution TEM image (Fig. S2). Both Al_2O_3 and nitrogen-doped graphene layers were coaxially deposited on CNTs, which was verified by energy-dispersive X-ray spectroscopy (Fig. S3). On the basis of aligned CNT templates, the resulting nitrogen-doped graphene/Al_2O_3/CNT also demonstrated high alignment confirmed by the dependence of electrical resistance on angle (Fig. S4). The Al_2O_3 layer was further thoroughly etched by HF solution to produce the hollow structure between CNT and nitrogen-doped graphene layer (Fig. 1d). Fig. S5 shows the nitrogen-doped graphene sheet peeled off the HNCNT, and it was flexible with well-maintained structure.

The parameters of the hollow structure can be well controlled by varying the thicknesses of Al_2O_3 and nitrogen-doped graphene layers (Fig. 2a). For instance, the size of the hollow structure was varied from 10 to 30 nm by controlling the thickness of Al_2O_3 from 10 to 30 nm (Fig. 2b–d and S6). As the lengths of HNCNTs were hundreds of micrometers, it remained challenging to accurately measure the specific surface area and pore distribution by the traditional method of measuring the typical nitrogen adsorption-desorption isotherms [22]. After etching the Al_2O_3 layer, the CNT template was observed randomly distributing within the inter-space. In addition, the thickness of the nitrogen-doped graphene layer can also be tailored, e.g., from 20 to 100 nm by increasing the re-growth time from 5 to 30 min (Fig. 2e and f, S7 and S8). It should be noted that occasionally more than one CNT had been bundled together within the nitrogen-doped graphene layer (Fig. S9). Besides, some cross-structured HNCNTs were also observed due to the crossed CNT templates (Fig. S10). Interestingly, more sophisticated hybrid structures can be synthesized on the basis of similar strategies. For instance, the deposition and growth of Al_2O_3 and nitrogen-doped graphene layers were repeatedly performed to form a Matryoshka-like structure. Both the Al_2O_3 and nitrogen-doped graphene layers had a thickness of ~20 nm, contributing to a total diameter of about 200 nm for the hybrid structure (Fig. S11), which was a magnitude larger than that of bare CNT. After complete removal of Al_2O_3, two hollow layers formed: one between CNT and the inner nitrogen-doped graphene layer, and the other sandwiched between two nitrogen-doped graphene layers (Fig. 2g).

The electrochemical properties of HNCNTs were investigated by assembling coin cells with lithium wafers as counter electrodes. It was found that the samples with 30 nm of Al_2O_3 layer and 5 min of

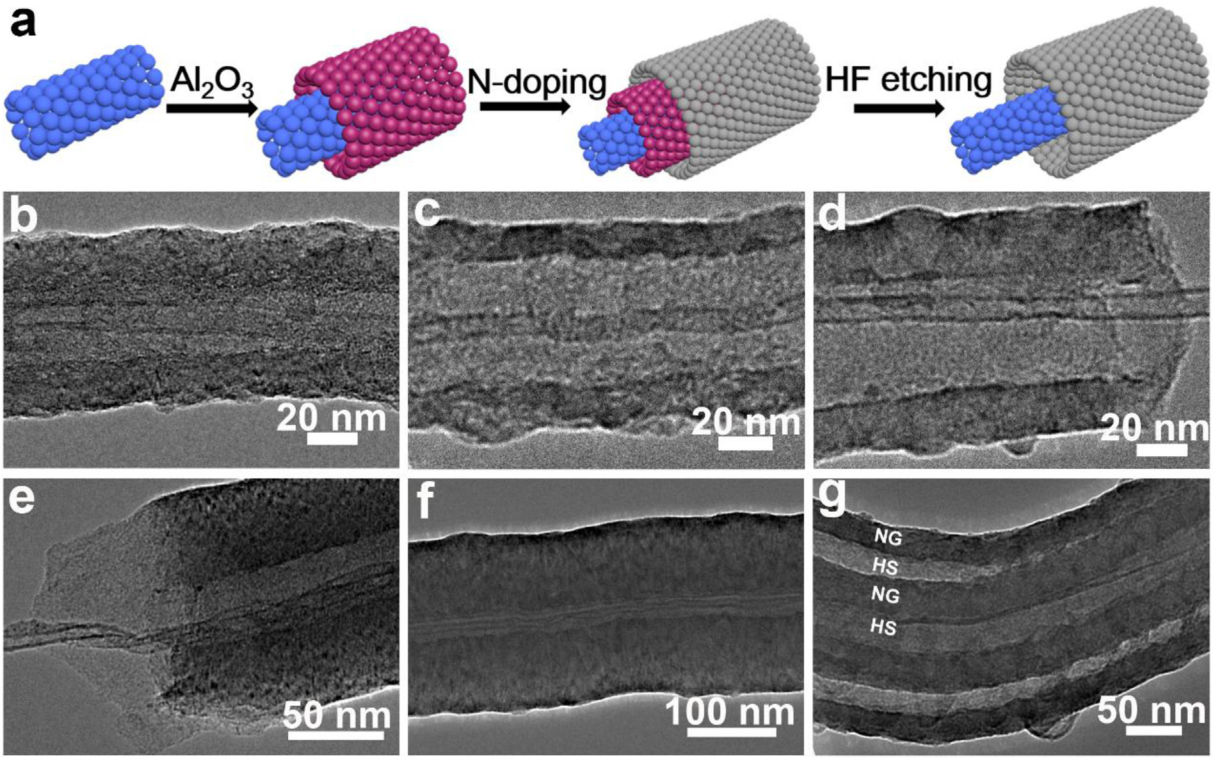

Fig. 2. (a) Schematic illustration to the HNCNT synthesis. (b–d) TEM images of nitrogen-doped graphene/Al_2O_3/CNT after HF etching with different Al_2O_3 thicknesses of 10, 20 and 30 nm, respectively. (e) and (f) TEM images of HNCNTs with different shell thicknesses of ~50 and ~100 nm, respectively. (g) HNCNTs with a "Matryoshka" structure containing two alternate Al_2O_3 and nitrogen-doped graphene layers. NG and HS in **g** represent nitrogen-doped graphene and hollow structure, respectively. (A colour version of this figure can be viewed online.)

re-growth time showed the highest specific capacity and had been used if not mentioned below. Cyclic voltammetry (CV) test showed irreversible capacity at the first cycle (Fig. 3a), mainly due to the formation of solid electrolyte interphase. The HNCNTs demonstrated a high discharge capacity of over 1500 mAh g^{-1} but a low coulombic efficiency of 50% (Fig. S12). The galvanostatic discharge took much more time than CV test, which enables effective diffusion of electrolyte and formation of more SEI films. After the first cycle, the coulombic efficiency reached over 80%. A capacity of 635 mAh g^{-1} was observed at the fifth cycle. As a comparison, nitrogen-doped graphene/CNT without the hollow structure in the wall displayed a much lower specific capacity of 360 mAh g^{-1} at the fifth cycle, indicating that the unique hollow structure can effectively increase the lithium storage capacity of CNTs.

The rate performance was further tested at different current densities (Fig. 3c). As the current density increased from 0.1 to 2 A g^{-1}, the discharge capacity decreased from 635 to 355 mAh g^{-1} and recovered to 540 mAh g^{-1} (85% of the initial value) when the current density returned to 0.1 A g^{-1}. The cyclic charge-discharge performances of HNCNTs were further measured at a current density of 2 A g^{-1}. Interestingly, an unexpected capacity increase was observed (Fig. S13), which was also found in the other N-doped carbon materials [23,24]. Li^+ intercalation and de-intercalation at the beginning resulted in a more disordered structure with more sites for Li^+ storage. The specific capacity increased from 320 to 900 mAh g^{-1} after 2000 charge-discharge cycles. On the contrary, a slow capacity decay was detected in the other samples with higher thicknesses of ~50 and ~100 nm, corresponding to the samples with re-growth time of 10 and 30 min, respectively (Fig. 3d and S14). It may be explained by the fact that the defects introduced by nitrogen-doping were favorable for the diffusion of Li^+ into the hollow structure, while thicker layers led to larger diffusion resistance for Li^+. The influence of the thicknesses of Al_2O_3 and nitrogen-doped graphene layer on specific capacity was further studied. HNCNTs with the thickest Al_2O_3 layer and thinnest nitrogen-doped graphene layer displayed the highest specific capacity (Fig. 3e). High Coulombic efficiencies above 90% were demonstrated for HNCNTs with a variety of thicknesses of Al_2O_3 and nitrogen-doped graphene layers, and the maximal value came to the samples with the thicknesses of 10 and 100 nm for Al_2O_3 and nitrogen-doped graphene layers, respectively (Fig. 3f).

The designed hollow structure had been verified as an efficient platform for lithium storage. The lattice of HNCNTs became fuzzy after discharging, indicating that Li^+ had diffused from the electrolyte into the inner space through the defects on nitrogen-doping graphene layer (Fig. S15). Furthermore, several lithium clusters can be observed within the hollow structure. In high-resolution TEM image, neat crystal lattice of lithium ions can be observed with an interplanar spacing of 0.24 nm which corresponded to uniformly distributed lithium ions. Therefore, a high specific capacity enhancement was produced for the HNCNTs with a re-growth time of 5 min (Fig. S16).

Note that HNCNTs can not only serve as promising anode materials for LIBs, but also as ideal hosts for incorporation of the other active materials. For instance, Si with a high theoretical specific capacity of 4200 mAh g^{-1} represents a promising candidate for high energy density anode material of LIBs [25–29]. However, the huge volume change during charge-discharge processes had largely hindered their applications towards high-performance LIBs [30–34]. Herein, Si was introduced to HNCNTs to further enhance the lithium storage performance (Fig. 4a). Si (50 nm) and Al_2O_3 (20 nm) were deposited on CNTs layer by layer, and another

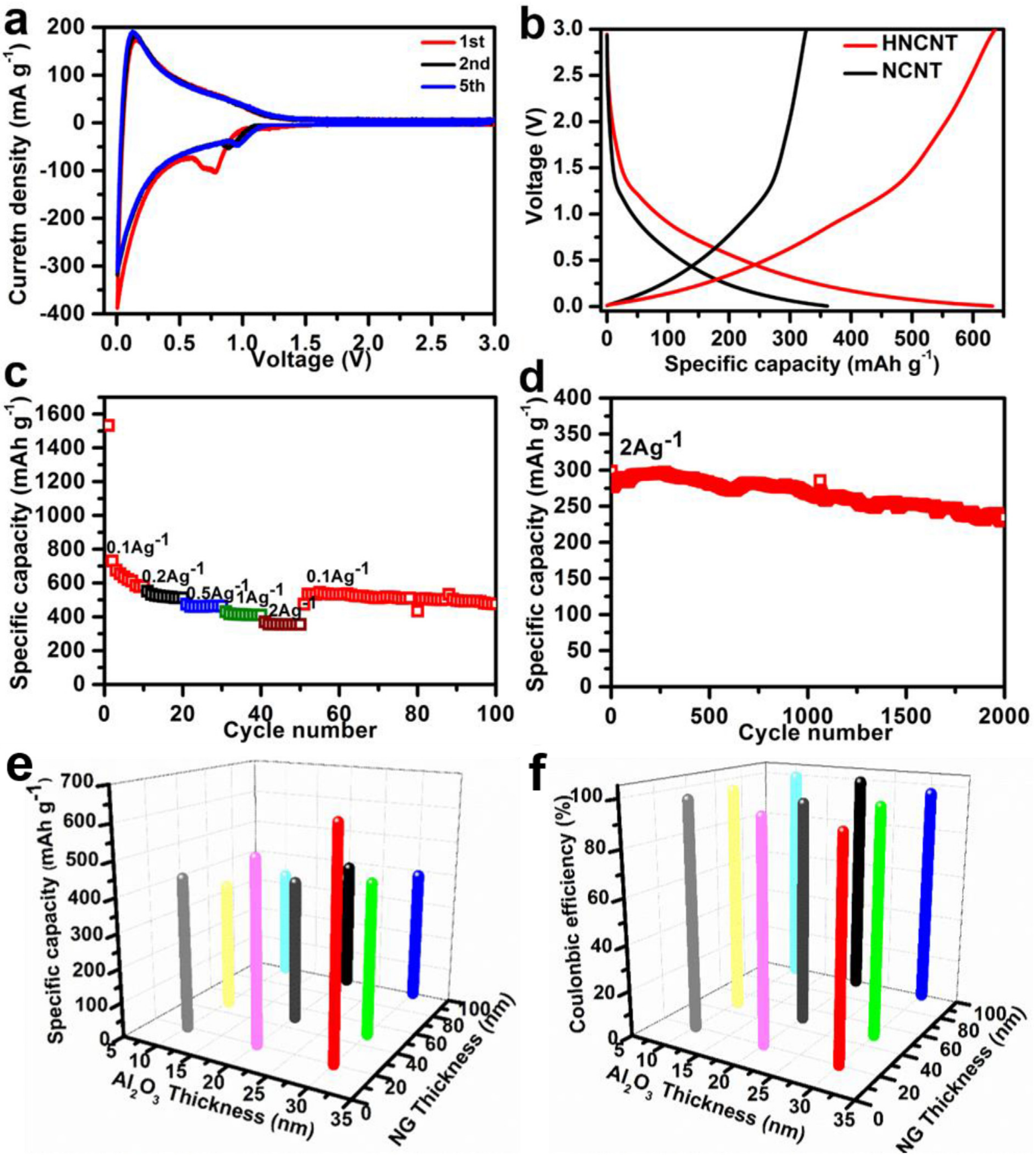

Fig. 3. Electrochemical properties of HNCNTs. (a) Cyclic voltammograms of HNCNTs at a scan rate of 0.5 mV/s (3.0–0.01 V). (b) Galvanostatic charge-discharge curves of nitrogen-doped CNT and HNCNTs in the 5th cycle. (c) Rate performance of HNCNTs. The thicknesses of Al$_2$O$_3$ and nitrogen-doped graphene layer in a-c are 30 and ~20 nm, respectively. (d) Long cycle stability of HNCNTs. Current densities in b and d are 0.1 and 2 A g^{-1}, respectively. The thicknesses of Al$_2$O$_3$ and nitrogen-doped graphene (NG) layer in d are 30 and ~50 nm, respectively. (e) Dependence of specific capacity on thickness of Al$_2$O$_3$ and nitrogen-doped graphene layer. (f) Dependence of Coulombic efficiency on thickness of Al$_2$O$_3$ and nitrogen-doped graphene layer. (A colour version of this figure can be viewed online.)

nitrogen-doped graphene layer (20 nm) was further grown outside (Fig. 4b). Here HCl was used in replacement of HF as the etching solution to avoid the etching of Si by HF (Fig. 4c and S17). The incorporation of Si resulted in a higher specific capacity of 930 mAh g^{-1} and lo5w discharge platform of 0.2 V (Fig. 4d). The Coulombic efficiency reached 90% since the second charge-discharge cycle. High rate performance was also demonstrated with 82.5% of the capacity retention when the current density increased from 0.1 to 2 A g^{-1} and returned to 0.1 A g^{-1} (Fig. 4e). The capacity was mainly limited by the expansion of Si. The effective volume for accommodating Si volume expansion $V_{hollow} = \pi (R_1^2 - R_2^2)$ *L, and the Si volume $V_{Si} = \pi (R_2^2 - R_3^2)$ *L, where R_1, R_2 and R_3 are the diameters of hollow structure (80 nm), silicon (60 nm) and CNT (10 nm), respectively. The ratio of V_{hollow} to V_{Si} was thus calculated as 80%, so Si may expand by 80%. As a result, the maximum capacity of Si was 4200 * (80%/280%) = 1200 mAh g^{-1}. Furthermore, 81% of the initial capacity had been maintained after 100 charge-discharge cycles at 2 A g^{-1} (Fig. S18). As a strong comparison, nitrogen-doped

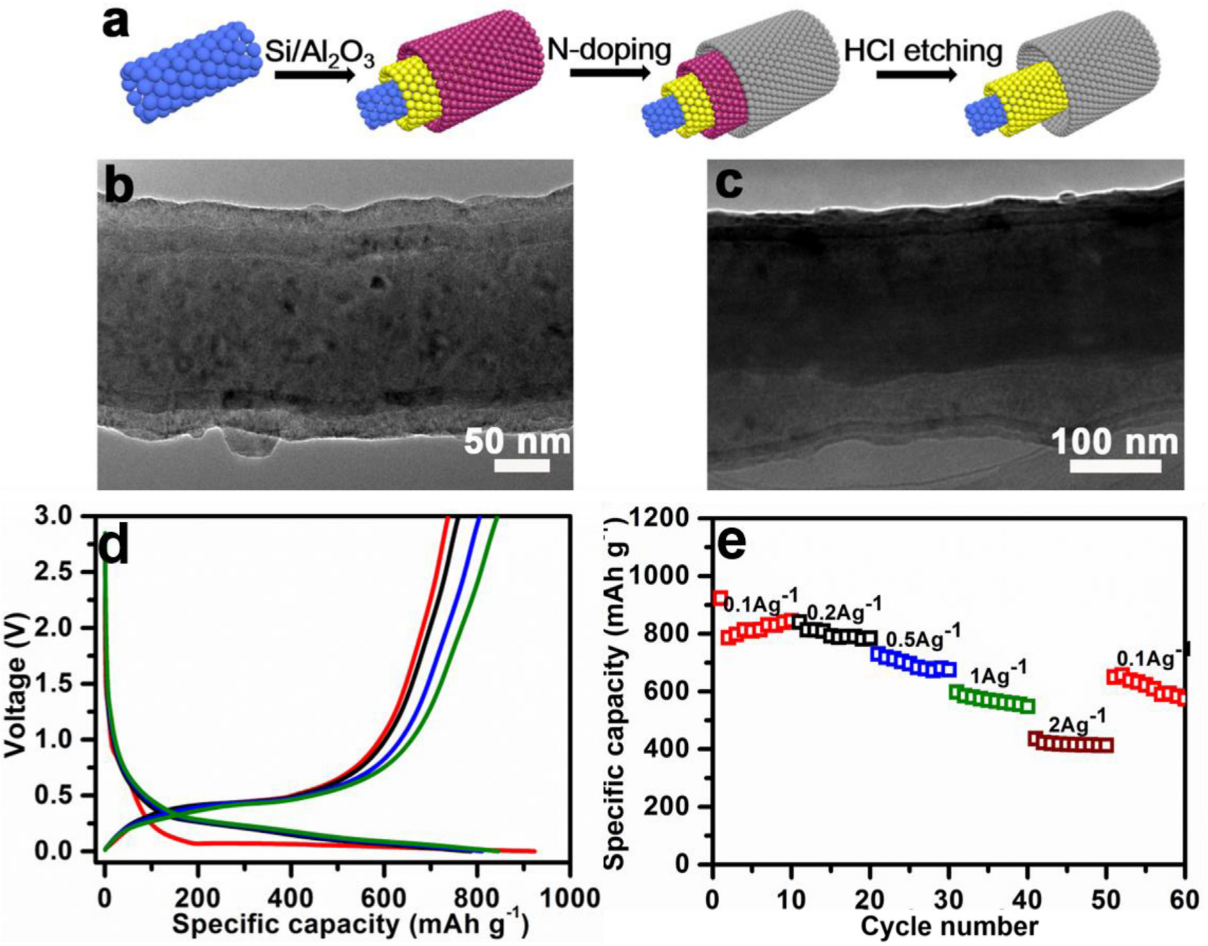

Fig. 4. (a) Schematic illustration to the synthesis of Si-incorporated HNCNTs. (b) and (c) TEM images of Si-incorporated HNCNTs before and after the formation of hollow structure. The thicknesses of Si and nitrogen-doped graphene layer are 50 and 20 nm, respectively. (d) Charge-discharge curves of Si-incorporated HNCNTs. (e) Rate performance of Si-incorporated HNCNTs. (A colour version of this figure can be viewed online.)

graphene/Si/CNT hybrids without the hollow structure demonstrated poor electrochemical performances (310 mAh g^{-1} at the beginning), because the nitrogen-doped graphene layer was too rigid to accommodate the large volume change of Si (Figs. S19 and S20).

The as-synthesized HNCNTs show several advantages compared with the other CNT-derived materials. Firstly, the hollow structure has been verified as a novel platform for efficient lithium storage, and an ideal host for incorporation of the other active materials to enhance the energy storage performances. Secondly, the lone pair electrons in nitrogen-doped graphene facilitates the electron transport process along the axial direction of CNTs. Thirdly, the active sites and defects introduced by nitrogen-doped graphene layers are beneficial for electrochemical property enhancement of the hybrids. Last but not the least, the alignment of HNCNTs largely decreases the contact resistance among CNTs, contributing to reduced inner resistance for the assembled devices.

4. Conclusion

In summary, a new family of CNTs with desired hollow walls had been synthesized. The unique hollow structure can be used for lithium storage and as host for other active materials. When Si was embedded to serve as anodes for LIBs, a high capacity of 930 mAh g^{-1} was achieved. This work presents a general and promising strategy in developing high-performance energy storage materials.

Acknowledgments

This work was supported by MOST (2016YFA0203302), NSFC (21634003, 51573027, 51403038, 51673043, 21604012) and STCSM (16JC1400702, 15XD1500400, 15JC1490200).

Appendix A. Supplementary data

Supplementary data related to this article can be found at https://doi.org/10.1016/j.carbon.2018.03.021.

References

[1] P. Simon, Y. Gogotsi, Materials for electrochemical capacitors, Nat. Mater. 8 (2008) 845–854.
[2] N. Yabuuchi, K. Kubota, M. Dahbi, S. Komaba, Research development on sodium-ion battery, Chem. Rev. 114 (2014) 11636–11682.
[3] G. Girishkumar, B. McCloskey, A.C. Luntz, S. Swanson, W. Wilcke, Lithium-air battery: promise and challenges, J. Phys. Chem. Lett. 1 (2010) 2193–2203.
[4] P.G. Bruce, S.A. Freunberger, L.J. Hardwick, J.M. Tarascon, Li-O$_2$ and Li-S batteries with high energy storage, Nat. Mater. 11 (2012) 19–29.
[5] H. Li, Z. Wang, L. Chen, X. Huang, Research on advanced materials for Li-ion batteries, Adv. Mater. 21 (2009) 4593–4607.
[6] Y. Liang, T. Tao, J. Chen, Organic electrode materials for rechargeable lithium batteries, Adv. Energy Mater. 2 (2012) 742–769.
[7] P. Roy, S.K. Srivastava, Nanostructured anode materials for lithium ion batteries, J. Mater. Chem. A 3 (2015) 2454–2484.

[8] Y. Zhang, W. Bai, J. Ren, W. Weng, H. Lin, Z. Zhang, et al., Super-stretchy lithium-ion battery based on carbon nanotube fiber, J. Mater. Chem. A 2 (2014) 11054–11059.

[9] Y. Wu, E. Rahm, B. Holze, Carbon anode materials for lithium ion batteries, J. Power Sources 114 (2003) 228–236.

[10] J. Ren, Y. Zhang, W. Bai, X. Chen, Z. Zhang, X. Fang, et al., Elastic and wearable wire-shaped lithium-ion battery with high electrochemical performance, Angew. Chem. Int. Ed. 53 (2014) 7864–7869.

[11] X. Li, J. Yang, Y. Hu, J. Wang, Y. Li, M. Cai, et al., Novel approach toward a binder-free and current collector-free anode configuration: highly flexible nanoporous carbon nanotube electrodes with strong mechanical strength harvesting improved lithium storage, J. Mater. Chem. 22 (2012) 18847–18853.

[12] Y. Chen, X. Li, K. Park, J. Song, J. Hong, L. Zhou, et al., Hollow carbon-nanotube/carbon-nanofiber hybrid anode for Li-ion batteries, J. Am. Chem. Soc. 135 (2013) 16280–16283.

[13] W. Weng, Q. Sun, Y. Zhang, S. He, Q. Wu, J. Deng, et al., A gum-like lithium-ion battery based on a novel arched structure, Adv. Mater. 27 (2015) 1363–1369.

[14] S.W. Lee, N. Yabuuchi, B.M. Gallant, S. Chen, B. Kim, P.T. Hammond, et al., Shao-Horn, High-power lithium batteries from functionalized carbon-nanotube electrodes, Nat. Nanotechnol. 5 (2010) 531–537.

[15] C. Kang, M. Patel, B. Rangasamy, K.N. Jung, C. Xia, S. Shi, et al., Three-dimensional carbon nanotubes for high capacity lithium-ion batteries, J. Power Sources 299 (2015) 465–471.

[16] Y. Dong, K. Md, Y.S. Chui, Y. Xia, C. Cao, J.M. Lee, et al., Synthesis of CNT@Fe_3O_4-C hybrid nanocables as anode materials with enhanced electrochemical performance for lithium ion batteries, Electrochim. Acta 176 (2015) 1332–1337.

[17] J.R. Dahn, Phase diagram of Li_xC_6, Phys. Rev. B 44 (1991) 9170–9177.

[18] A. Satoh, N. Takami, T. Ohsaki, Electrochemical intercalation of lithium into graphitized carbons, Solid State Ionics 80 (1995) 291–298.

[19] K. NIshidate, M. Hasegawa, Energetics of lithium ion adsorption on defective carbon nanotubes, Phys. Rev. B 29 (1997) 1–20.

[20] J. Zhao, A. Buldum, J. Han, J. Lu, First-principles study of Li-intercalated carbon nanotube ropes, Phys. Rev. Lett. 85 (1999) 1706–1709.

[21] Z. Zhang, Y. Zhang, Y. Li, H. Peng, The advancement of fiber-shaped energy harvesting and storage devices, Acta Polym. Sin. 0 (2016) 1284–1299.

[22] A. Peigney, Ch Laurent, E. Flahaut, R.R. Bacsa, S. Mahurin, A. Rousset, Specific surface area of carbon nanotubes and bundles of carbon nanotubes, Carbon 39 (2001) 507–514.

[23] B. Guo, X. Sun, G. Veith, Z. Bi, S. Mahurin, C. Liao, et al., Nitrogen-enriched carbons from alkali salts with high coulombic efficiency for energy storage applications, Adv. Energy Mater. 3 (2013) 708–712.

[24] X. Li, D. Geng, Y. Zhang, X. Meng, R. Li, X. Sun, Superior cycle stability of nitrogen-doped graphene nanosheets as anodes for lithium ion batteries, Electrochem. Commun. 13 (2011) 822–825.

[25] L. Zhang, R. Rajagopalan, H. Guo, X. Hu, S. Dou, H. Liu, Lithium-ion batteries: a green and facile way to prepare granadilla-like silicon-based anode materials for Li-ion batteries, Adv. Funct. Mater. 26 (2016), 468–468.

[26] W. Weng, H. Lin, C. Chen, J. Ren, Z. Zhang, L. Qiu, et al., Flexible and stable lithium ion batteries based on three-dimensional aligned carbon nanotube/silicon hybrid electrodes, J. Mater. Chem. A 2 (2014) 9306–9312.

[27] X. Han, H. Chen, X. Li, J. Wang, C. Li, S. Chen, et al., Interfacial nitrogen stabilizes carbon-coated mesoporous silicon particle anodes, J. Mater. Chem. A 4 (2016) 434–442.

[28] S.H. Ng, J. Wang, D. Wexler, K. Konstantinov, Z.P. Guo, H.K. Liu, Highly reversible lithium storage in spheroidal carbon-coated silicon nanocomposites as anodes for Lithium-ion batteries, Angew. Chem. Int. Ed. 45 (2006) 6896–6899.

[29] H. Kim, J. Cho, Superior lithium electroactive mesoporous Si@carbon core-shell nanowires for lithium battery anode material, Nano Lett. 8 (2008) 3688–3691.

[30] L. Cui, Y. Yang, C.M. Hsu, Y. Cui, Carbon-silicon core-shell nanowires as high capacity electrode for lithium ion battery, Nano Lett. 9 (2009) 3370–3374.

[31] N. Liu, H. Wu, M.T. McDowell, Y. Yao, C. Wang, Y. Cui, A yolk-shell design for stabilized and scalable Li-ion battery alloy anodes, Nano Lett. 12 (2012) 3315–3321.

[32] A. Magasinski, P. Dixon, B. Hertzberg, A. Kvit, J. Ayala, G. Yushin, High-performance lithium-ion anodes using a hierarchical bottom-up approach, Nat. Mater. 9 (2010) 353–358.

[33] C.K. Chan, H. Peng, G. Liu, K. Mcilwarth, X. Zhang, R.A. Huggins, et al., High-performance lithium battery anodes using silicon nanowires, Nat. Nanotechnol. 3 (2007) 31–35.

[34] X. Su, Q. Wu, J. Li, X. Xiao, A. Lott, W. Lu, et al., Silicon-based nanomaterials for lithium-ion batteries: a review, Adv. Energy Mater. 4 (2014) 375–379.